Environmental Science Nano

Accepted Manuscript

This article can be cited before page numbers have been issued, to do this please use: M. Morataya-Reyes, A. Villacorta, J. Arribas-Arranz, J. Martín- Pérez, J. F. Ferrer, S. Pastor, R. Egea, I. Barguilla, R. Marcos and A. Hernández Bonilla, *Environ. Sci.: Nano*, 2025, DOI: 10.1039/D5EN00434A.

ROYAL SOCIETY OF CHEMISTRY

rsc.li/es-nano

DOI: 10.1039/D5EN00434A

Environmental Implication

Micro/nanoplastics, as new emergent environmental contaminants, can affect human health. Since the induced harmful effects can correlate with internalization, it is necessary to understand the internalization mechanisms and the potential correlations between internalization and induced effects. To solve these points, pristine polystyrene nanoplastics and true-to-life nanoplastics, derived from plastic goods and pellets, were evaluated. Results indicate the polymeric nature and surface charge are relevant factors modulating internalization. Furthermore, internalization does not correlate with the induce effects, polyethylene terephthalate (PET) and polylactic acid (PLA) true-to-life nanoplastics inducing stronger effects. This highlights the importance of using environmentally representative MNPLs to better assess the health risks associated with environmental MNPL exposure.

Exploring the impact of nanoplastics on human hepatic cells: dynamics of internalization and harmful effects in HuH-7 cells

Michelle Morataya-Reyes[1], Aliro Villacorta[1,2], Jessica Arribas Arranz[1], Joan Martín- Pérez[1], Juan Francisco Ferrer[3], Susana Pastor[1], Raquel Egea[1], Irene Barguilla[1], Ricard Marcos[1], Alba Hernández[1,*]

[1]Group of Mutagenesis, Department of Genetics and Microbiology, Faculty of Biosciences, Universitat Autònoma de Barcelona, Cerdanyola del Vallès (Barcelona), Spain.

[2]Facultad de Recursos Naturales Renovables, Universidad Arturo Prat, Iquique, Chile.

[3]AIMPLAS, Plastics Technology Center, Valencia Parc Tecnològic, 46980 Paterna, Spain.

[*]Corresponding author at Group of Mutagenesis, Department of Genetics and Microbiology, Faculty of Biosciences, Universitat Autònoma de Barcelona, Campus of Bellaterra, 08193 Cerdanyola del Vallès (Barcelona), Spain.

E-mail: alba.hernandez@uab.cat (A. Hernández)

DOI: 10.1039/D5EN00434A

Abstract

The increasing prevalence of micro- and nanoplastics (MNPLs) in the environment necessitates a detailed examination of their potential health impacts and the factors influencing these responses. Since internalization is a prerequisite for inducing adverse effects, we investigated the roles of surface modifications and polymer composition in human liver cells (HUH-7). Our study compared the internalization and effects of a pristine polystyrene nanoplastic (PS50-NPLs), two carboxylated polystyrenes of different sizes (cPS50-NPLs and cPS100-NPLs), and two environmentally relevant nanoplastics derived from polyethylene terephthalate water bottles (PET-NPLs) and polylactic acid pellets (PLA-NPLs). Significant variations in cell internalization were observed, with cPS50-NPLs and PET-NPLs showing the highest levels, and PS50-NPLs showing the lowest. Interestingly, internalization alone did not correlate directly with the induced effects; only PET-NPLs and PLA-NPLs induced reactive oxygen species (ROS), genotoxicity, and increased cytokine release. These results suggest that while internalization is essential in assessing MNPL toxicity, harmful effects also depend on other particle characteristics. The notable impact of the realistic environmental models PET-NPLs and PLA-NPLs underscores the importance of using environmentally representative MNPLs to better assess the health risks associated with environmental MNPL exposure.

Keywords: HUH-7 cells; nanoplastics; internalization; hazardous effects; surface modifications

1. Introduction

The exponential increase in plastic production and usage, particularly over the last decade, has brought significant advantages but also serious waste management challenges (Geyer et al., 2017). When used, improperly disposed of, or recycled plastics degrade in the environment through mechanical wear, photo-oxidation, hydrolysis, and microbial action, leading to the formation of microplastics (MPLs, 1-1000 μm) and nanoplastics (NPLs, 1-1000 nm) (Pradel et al., 2023). This constant degradation results in a range of particle sizes, often referred to as environmental secondary micro/nanoplastics (MNPLs) due to their continuous breakdown in natural environments.

The minute size of NPLs imparts them with unique physicochemical properties, enhancing their mobility and bioavailability across various environmental settings (Materic et al., 2022; Vasse and Melgert, 2024). Characteristics such as Brownian motion, high surface reactivity, additive leachate potential, and the ability to traverse physiological barriers make these particles a particular concern for human health researchers (Pradel et al., 2023). MNPLs have been detected in numerous consumables, including food and water (Wright and Kelly, 2017; Paul et al., 2020; Banaei et al., 2023), and have even been identified in human excretions, such as stool and urine (Schwabl et al., 2019; Pironti et al., 2023), confirming exposure through diet. Their presence in lung tissue also suggests inhalation exposure (Chen et al., 2020; Jenner et al., 2022). While the exact internal dose of these particles remains under investigation (Ali et al., 2024), studies have shown that MNPLs can migrate into the bloodstream and reach remote organs, including the heart and placenta (Ragusa et al., 2021; Alqahtani et al., 2023; Marfella et al., 2024).

The liver, a critical organ for metabolic regulation and detoxification, is particularly vulnerable to NPLs (Ge et al., 2023). In human liver samples from individuals with cirrhosis, MNPLs of various polymers have been identified, unlike in healthy individuals where no such particles were detected (Horvatits et al., 2022). Animal models similarly

View Article Online
DOI: 10.1039/D5EN00434A

demonstrate MNPL accumulation in the liver, as observed in fish (Zitouni et al., 2021) and mice (Fan et al., 2022) following oral administration of polystyrene nanoplastics (PS-NPLs).

Research using animal models and *in vitro* approaches has revealed the detrimental effects of NPLs on hepatic cells, including internalization, cytotoxicity, oxidative stress, and disturbed cellular homeostasis in various liver cell lines, such as HepG2 (He et al., 2020) and HL7702 (Shen et al., 2022). However, the precise mechanisms underlying NPL-induced hepatotoxicity remain unclear. Furthermore, most studies have focused solely on PS-NPLs of similar sizes and characteristics, which may not accurately reflect the diverse composition of secondary MNPLs found in the environment.

For a more comprehensive understanding of the effects and mechanisms of action of MNPLs on human liver cells, toxicological evaluations should use materials closely resembling those found in real-world environments, varying in size, surface properties, polymer type, and shape (Martin et al., 2022). These realistic analogs, termed true-to-life MNPLs, serve as models for environmental secondary MNPLs (Mills et al., 2023).

In this study, we examined the dynamics of internalization and effects of five distinct NPLs on HUH-7 hepatic cells. The NPLs selected include three commercial PS-NPLs (one pristine, and two carboxylated of varying sizes) and two environmentally representative NPLs derived from polyethylene terephthalate (PET) and polylactic acid (PLA). By incorporating a variety of polymers, sizes, and surface modifications, we aim to elucidate how these factors influence the hepatotoxic potential of MNPLs.

2. Materials and methods

2.1. NPLs characterization

PS-NPLs (Spherotech, PP008-10), cPS50-NPLs (Polysciences, Inc., 15913-10), cPS100-NPLs (Polysciences, Inc., 16688-15), and their respective fluorescent counterparts f-PS-NPLs (Spherotech, FP-00552-2 ex: 460 nm, em: 480 nm), f-cPS50-NPLs (Polysciences, Inc., 16661-10 ex: 441 nm, em: 486 nm), f-cPS100-NPLs (Polysciences, Inc., 16662-10 ex: 441 nm, em: 486 nm) were purchased from the indicated sources. Realistic environmental model NPLs were in-house obtained from plastic water bottles or pellet degradation, as described in Villacorta et al. (2022) for PET-NPLs and in Alaraby et al. (2024) for PLA-NPLs. Their fluorescent counterparts were prepared following a labelling protocol based on the use of a regularly used textile dye, iDye polypink (Jacquard Products, Healdsburg, CA, USA) (Villacorta et al., 2023, 2024) and 5(6)-FAM (Alaraby et al., 2024), respectively. After staining, particles were subjected to ultrafiltration and multiple washing steps to remove unbound dye. The absence of fluorescence in the final wash was used to confirm effective dye removal. The cytocompatibility of these labeled particles was previously validated by Villacorta et al. (2024), who reported no additional cytotoxic effects from the labeled NPLs, compared to unlabeled controls.

Size and shape were determined by transmission electron microscopy (TEM) using a JEOL JEM 1400 instrument (JEOL LTD, Tokyo, Japan) at 120 kV operation settings. Particles for TEM were prepared by placing a 7 µL drop of particle suspension at a concentration of 200 µg/mL on a carbon covered cooper grid, let dry overnight inside a covered petri dish. For all particles in suspension the size distribution was determined by dynamic light scattering (DLS), using a Zetasizer® Ultra device from Malvern Panalytical (Cambridge, United Kingdom). Working particle suspensions were prepared at concentration of 100 µg/mL. Once sonicated, size was determined by transferring 1 mL of particle suspension on independent DTS0012 cuvettes and performing the

experiments by triplicate using refractive indexes of 1.59, 1.47, and 1.57 for PS, PLA and, PET respectively. For ζ-potential a similar approach was done but the measurements were carried out on DTS1070 cuvettes. Parallelly, from the same suspensions the particle size was also determined by a combination of light scattering and Brownian movement on a Nanosight NS300 nanotracking analysis from Malvern Panalytical Ltd (Cambridge, United Kingdom). To assess the chemical composition of the true-to-life PET- and PLA-NPLs, FTIR analyses were carried out. To proceed, we used the protocols previously described (Villacorta et al., 2022; García-Rodriguez et al., 2024) and the previously reported characteristic polymer spectral bands (Nazrin et al 2020; Johnson et al 2021).

2.2. Cell culture conditions

HUH-7 cells obtained from JCRB Cell Bank (JCRB0403) were used for the study. Cells were grown in Dulbecco's modified Eagle's medium (DMEM, Life Technologies, NY, USA) supplemented with 10% fetal bovine serum (FBS, Biowest, France), and 2.5 µg/mL of Plasmocin (InvivoGen, CA, USA). For HUH-7 passage, TrypLE™ Select Enzyme (1X) (Thermo Fisher Scientific, Waltham, MA) was used to detach cells. Cells were maintained in a 5% CO_2 humidified atmosphere at 37 °C.

2.3. Cell viability

To determine the sub-toxic concentrations of the different NPLs in HUH-7 cells, $1x10^5$ cells/well were seeded in triplicate in 12-well plates in a final volume of 1 mL of DMEM and treated with NPLs at concentrations from 0 to 200 µg/mL for 48 h. Cells were detached and cell number was determined using the LUNA-II™ Automated Cell Counter (Biocat, Heidelberg, Germany) in a 1:1 dilution with trypan blue (Sigma-Aldrich, St. Louis, MO). Each concentration average cell number was normalized against the average of the non-treated cells, and fold change was compared.

2.4. Determination of NPLs internalization in HUH-7 by confocal microscopy

To confirm NPLs internalization in HUH-7 cells, $1x10^4$ cells/well were seeded in an µ-Slide 8 well chambered coverslip (Ibidi GmbH, Gräfelfing, Germany) and treated with 100 µg/mL of the fluorescent/labeled NPLs (f-NPLs) for 48 h. Before observation with a Leica TCS SP5 confocal microscope, cells were washed with growth medium and Hoechst 33342 (ex: 405 nm, em: 415–503) and Cellmask (ex: 633 nm, em: 645–786) markers were added to stain the cell nuclei and cell membranes, respectively.

2.5. NPLs internalization in HUH-7 by flow cytometry

To determine the proportion of cells that internalize the different NPLs, $1x10^5$ cells/well were seeded in triplicate in 12-well plates in a final volume of DMEM with 100 µg/mL of the fluorescent/dyed NPLs. After treatment (1, 3, 24, 48, and 72 h), cells were detached and analyzed using a flow cytometer (CytoFLEX FACS from Beckman Coulter, Pasadena, CA, USA). After scoring 10,000 single cells, the percentage of cells that internalized the NPLs (fluorescent cells) and the mean intensity of the fluorescent signal were determined using CytExpert software.

2.6. ROS levels in HUH-7 cells that internalized NPLs

Production of ROS in HUH-7 cells after NPLs internalization was determined by the dihydroethidium (DHE, Calbiochem, USA) assay and measured using a flow cytometer Cytoflex S device (Beckman Coulter CytoFLEX S). A total of $1x10^5$ cells/well were seeded in triplicate in 12-well plates in a final 1 mL of DMEM volume and treated with 100 µg/mL of the different f-NPLs for 1, 3, 24, 48, and 72 h. After detaching, cells were centrifuged at 1200 rpm for 8 min and the medium was removed and replaced with PBS 1X. DHE solution was added to a final concentration of 1 µg/mL and the cell suspension was incubated for 30 min at 37 °C. DHE signal was determined by flow cytometry using the CytExpert software in 10,000 single cells of the treated population, and in the 10%

View Article Online
DOI: 10.1039/D5EN00434A

showing the highest internalization. ROS level in NPLs-treated cells was normalized against non-treated mean, for comparison.

2.7 DNA damage detected by the comet assay

Genotoxic and oxidative DNA damage in HUH-7 cells after 48 h of exposure to NPLs was evaluated using the comet assay, as described (Collins et al., 2023). To proceed, $1.5x10^5$ cells/well were seeded in duplicate in 12-well plates and treated with the selected NPLs for 48 h. After the exposure time, cells were washed with PBS 1X, trypsinized using TrypLE™ Select Enzyme (1X), collected, and centrifuged at 300 rcf for 8 min at 4 °C. After the supernatant was removed, cells were resuspended in cold PBS at a density of $1x10^6$ cells/mL, diluted (1:10) in 0.75% low melting point agarose at 37 °C and 7 µL drops of the mix were placed on Gelbond® films (GF, Life Sciences, Vilnius, Lithuania). Every treatment, and its duplicates, was represented with three drops each, and two GF with the same set of samples were processed in parallel. Cell lysis was done by submerging the GF in a cold lysis buffer for 2 h, at 4 °C. GFs were then washed twice for 5 min with cold enzyme buffer and later submerged for 50 min in the same buffer. A second incubation, with previously activated formamidopyrimidine DNA glycosylase (FPG) enzyme, was done at 37 °C for 30 min while the second identical GF was incubated in the same conditions without the enzyme. These GFs were then washed with electrophoresis buffer and then submerged in the same buffer for 25 min, allowing for DNA to unwind before electrophoresis (20 V, 300 mAmp, 25 min). After two washes with cold PBS, the GFs were fixed in absolute ethanol and stained with SYBR Gold (1:2,500) (TermoFisher Scientitic, Waltham, MA) in TE buffer (10 mM Tris Base, 1 mM EDTA; pH 8). Comets in the films were scored using an Olympus BX50 microscope at 20× magnification and the DNA percentage in the tail was recorded using the Komet 5.5 Image analysis system (Kinetic Imaging Ltd, Liverpool, UK). For genotoxic and oxidative DNA damage, methyl methane sulfonate (MMS) and potassium bromate ($KBrO_3$) were used as positive controls, respectively.

View Article Online
DOI: 10.1039/D5EN00434A

2.8. Cytokine expression

To determine differences in cytokines expression in HUH-7 cells exposed to NPLs (regarding the control), the Proteome Profiler Human Cytokine Array Kit (Bio-Techne R&D Systems, ARY005B. Minneapolis, MO), which detects 36 human cytokines, chemokines, and acute phase proteins simultaneously, was used. A total of $1x10^6$ cells were seeded in a 75 cm^2 flask and treated with 100 µg/mL of different NPLs for 48 h. Cell culture supernatant and cell lysate for each treatment were collected and incubated with the nitrocellulose membrane containing anti-cytokine antibodies, following the manufacturer's instructions. After detecting chemiluminescence from the membrane using ChemiDoc XRS+ System (BioRad, Alcobendas, Spain), the average pixel density of the pair of spots representing each cytokine was determined using the ImageJ program.

To determine the effect of inflammation stimulus, in cells previously exposed to NPLs, cells were exposed to the fluorescent version of PET- and PLA-NPLs for 48 h and cells were sorted using fluorescence-activated cell sorting (FACS) to separate the 50% of the population showing the highest internalization. After seeding these cells, they were treated with lipopolysaccharide (LPS) at 1 µg/mL for 12 h and differences in cytokines expression were determined using the previously described method. These profiles were compared to those of HUH-7 cells treated with LPS for 12 h after 48 h of incubation without NPLS.

2.9. Statistical analysis

Data was analyzed using the GraphPad Prism Software 7.0 (GraphPad, San Diego, CA). HUH-7 cells after treatment with the different NPLs were compared against non-treated cells using the one-way ANOVA with Dunnett multiple comparisons post-test, and a confidence interval of 95% (n=3).

View Article Online
DOI: 10.1039/D5EN00434A

3. Results and discussion

3.1. NPL characterization

The maintenance of nanometric-scale characteristics in plastic particle suspensions is crucial for accurately assessing their hazard potential. Therefore, we have adopted an approach aligned with the recommendations of the European Commission (European Commission, 2022), focusing on their size characteristics in the dry state while also evaluating their behavior in suspension. For their dry-state characteristics, we followed previously reported guidelines (Arribas Arranz et al., 2024; Domenech et al., 2024). The shape and size, as assessed by TEM, confirmed a spherical-like morphology for commercially designed particles intended to retain this structure as observed in Fig 1 (a, d, g). Their size distribution was characterized by measuring the Martin diameter of a minimum of 100 nanoparticles, yielding an average size of 76.45 ± 0.02 nm for PS50-NPLs, 46.65 ± 0.01 nm for cPSC50-NPLs, and 97.51 ± 8.64 nm for cPSC100-NPLs. Additionally, the polydispersity index remained consistently low across all samples, recorded at 0.03, 0.04, and 0.01 for PS50-, cPSC50-, and cPSC100-NPLs, respectively. These results are in line with those observed by DLS and NTA, all summarized in supplementary Tables S1 and S2, respectively. The little variation in size can be attributed to the high charge of the particles which in all cases for the engineering nanoparticles, the ζ-potentials were higher than -40 mV and therefore the particles in the suspension can be considered stable in terms of electrostatic repulsion (Onugwu et al., 2023). In the electron microscopy analysis, we determined that PET-NPLs exhibit high heterogeneity in terms of particle shape and size (Fig. 1j), which can be considered as a desirable feature when it comes to environmentally representative nanoplastics. However, the submicrometric fraction displays a distribution in which 98.8% of particles are below 500 nm, while the fraction of agglomerates exceeding 1 µm represents only 0.5% of the sample. Consequently, the average particle size in suspension is 176.24 ± 6.52 nm, with hydrodynamic behavior ranging from 200 to 300 nm (Fig. 1j-l). This

View Article Online
DOI: 10.1039/D5EN00434A

particle-by-particle behavior, with a small fraction exceeding 500 nm, is evident in Fig. 1k, where the NTA values align with the size description obtained through TEM. This heterogeneity mimics how real-world nanoplastics derived from environmental degradation are unlikely to retain uniform and spherical shapes. Instead, environmental nanoplastics are expected to display a range of irregular forms, surface textures, and sizes due to long-term exposure to mechanical abrasion, photo-oxidation, and chemical weathering (Zhang et al., 2020; Enfrin et al., 2020). Although high-resolution nanoscale characterization of field-collected nanoplastics remains technically limited, emerging studies have documented the presence of polydisperse, non-spherical, and fragmented plastic particles in environmental samples (Kooi and Koelmans, 2019; Catarino et al., 2023). This contrasts with the use of commercially available, monodisperse polystyrene beads, which dominate nanotoxicology literature but may not fully reflect the diversity of particles that organisms are exposed to in real environmental settings.

View Article Online
DOI: 10.1039/D5EN00434A

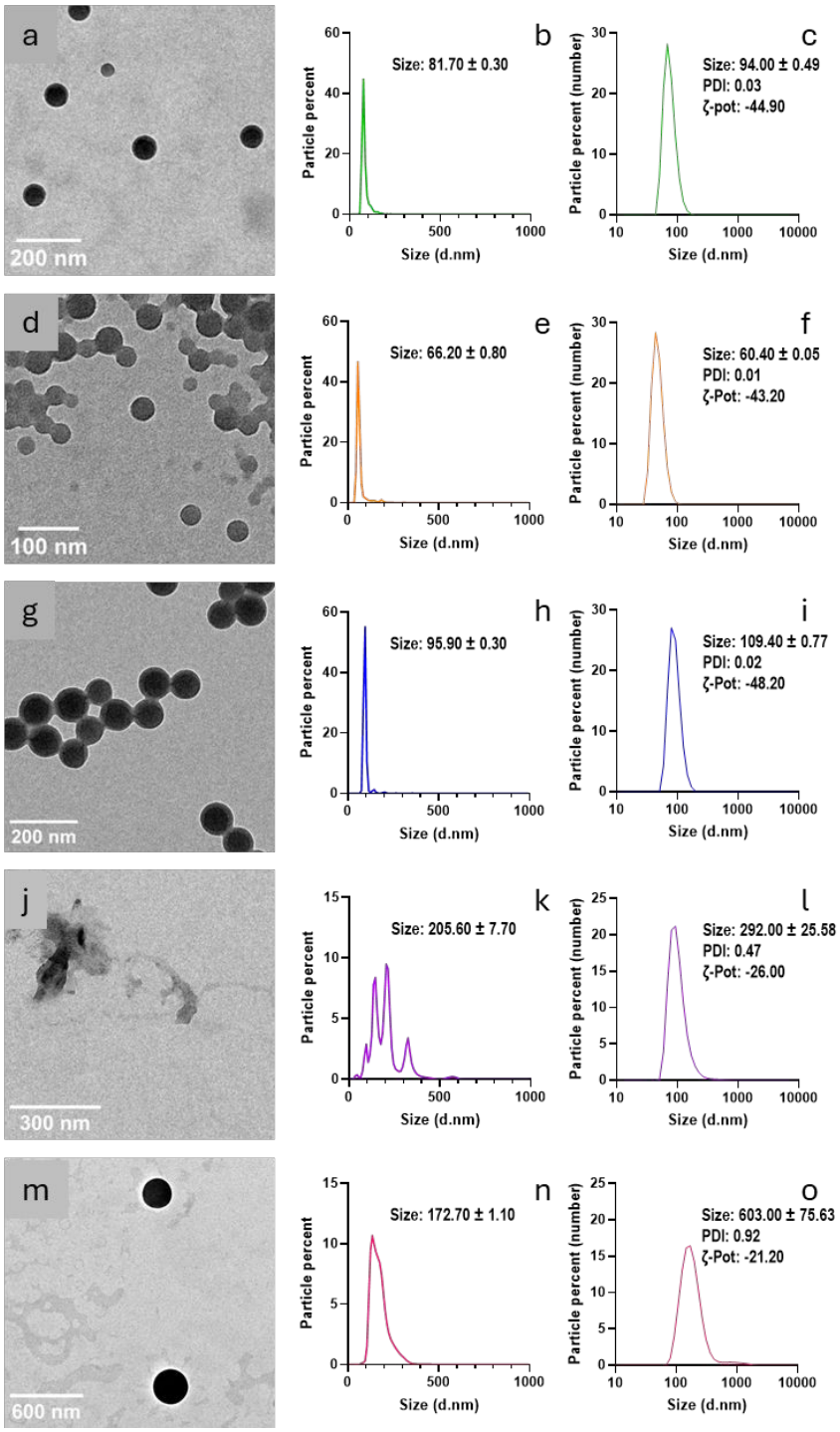

Figure 1. TEM representative images for PS (a), cPS50 (d), cPS100 (g), PET (j), and PLA (m) NPLs. NTA analysis for the selected NPLs shows a narrow size distribution for PS (b), cPS50 (e), and cPS100 (h), while broader peaks are shown for PET (k) and PLA (n). It is remarkable that multimodal peaks are present for PETNPLs. Hydrodynamic behavior for PS50 (c), cPS50 (f), cPS100 (i), PET (l), and PLA (o) NPLs.

Regarding suspension stability, the ζ-potential values are near the stability threshold, averaging -26 mV, suggesting that these particles remain relatively stable in suspension. For PLA-NPLs (Fig. 1m-o), the size distribution determined by microscopy is 129.76 ±

1.40 nm, while NTA gives a mean of approximately 172.70 ± 1.10 nm; however, DLS values increase to 603.00 ± 75.63 nm, with a polydispersity index (PDI) that, while low, is the highest among the suspensions analyzed. This discrepancy may be attributed to a reasonably adequate ζ-potential of -21.20 mV which, while relatively good, is not on the range of stability zone (>± 30 mV). While excessive agglomeration should not occur, it is well-known that the DLS technique is sensitive to agglomeration occurrences, and their presence can lead to reading errors (Bhattacharjee, 2016). The full description of true-to-life PET- and PLA-NPLs for both DLS and NTA values are summarized in supplementary Tables S1 and S2, respectively. To confirm the chemical composition of the true-to-life PET- and PLA-NPLs, the obtained FTIR interferograms (Fig. S1) were analysed and contrasted with the representative bands reported in previous studies. The obtained peaks match well with the expected, confirming the PET and PLA nature of the used NPLs.

3.2. NPL toxicity

The human hepatoma-derived HuH-7 cell line is a widely accepted experimental model for studying liver responses, as a substitute for primary hepatocytes (Jouan et al., 2016). Understanding hepatocyte immune responses to nanoplastics (NPLs) is crucial for clarifying the pathogenesis of NPL-induced liver injury and the broader implications for global health. Hepatocytes play a dual role in immune regulation, acting as both targets and effectors. Recent evidence suggests that NPLs can activate innate immune pathways in hepatocytes, leading to the release of pro-inflammatory cytokines and chemokines. Additionally, NPLs may influence adaptive immune responses through interactions with antigen-presenting cells within the liver microenvironment (Wang et al., 2024).

Our findings highlight the notable variation in cellular responses to different nanoplastic types within the same hepatic cell line. Although we observed no direct cytotoxicity (as measured by cell viability), both PLA- and PET-NPLs significantly

View Article Online
DOI: 10.1039/D5EN00434A

impacted ROS production, genotoxicity, and cytokine expression in HUH-7 cells, suggesting their potential to induce sub-lethal damage.

Initially, we evaluated HUH-7 cell viability following 48-h exposures to PS-NPLs, carboxylated PS-NPLs (two sizes), PET-NPLs, and PLA-NPLs at concentrations of 50, 100, and 200 µg/mL (Fig. 2). No significant differences in cell viability were observed across all treatments compared to the control, indicating that short-term exposure to these NPLs does not induce cytotoxicity at the tested concentrations. This lack of an immediate cytotoxic effect could reflect either a resistance specific to this cell line or align with previous studies on nanoplastics, where direct cell death is often absent despite cellular disturbances such as oxidative stress or genotoxicity (Shi et al., 2021; Khan and Jia, 2023; Tavakolpournegari et al., 2023).

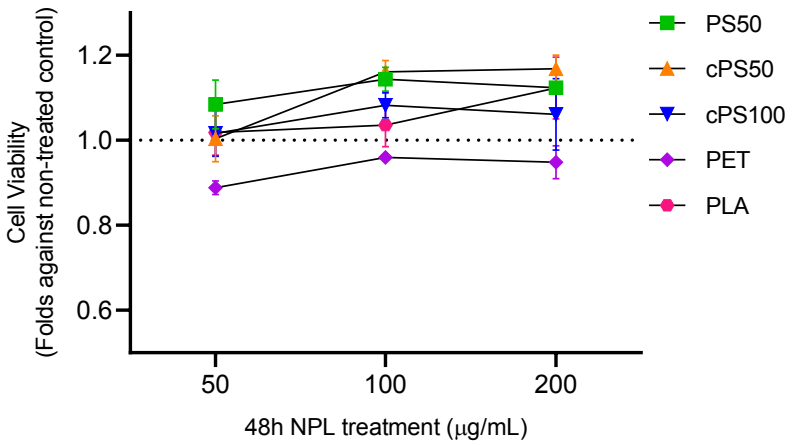

Figure 2. HUH-7 cell viability after 48 h of treatment with NPLs at 50, 100, and 200 µg/mL. No significant differences were observed after comparing the fold in cell number of treated cells against the number in the non-treated control when using one-way ANOVA, with Dunnett multiple comparisons post-test and a confidence interval of 95%. Graph represents mean ± SEM fold change against the untreated control (n=3).

While the concentrations of NPLs used in this study are higher than current estimates of environmental exposure levels, this approach is consistent with numerous *in vitro* toxicological studies aimed at uncovering mechanistic insights into cellular responses to these particle exposures. The use of higher concentrations is a well-established strategy

View Article Online
DOI: 10.1039/D5EN00434A

to amplify biological signals in a controlled system, and to identify potential pathways of toxicity, especially when investigating emerging contaminants like NPLs, for which standardized exposure metrics and chronic low-dose data are still evolving (Yee et al., 2021; Sendra et al., 2021). Moreover, quantifying environmentally relevant internal doses of nanoplastics remains challenging due to variability in particle size, composition, and lack of consensus on exposure metrics (Vethaak and Legler, 2021). Previous studies have detected MNPLs in human tissues, including lungs, placentas, blood, and even liver samples, confirming human exposure despite low environmental concentrations (Ragusa et al., 2021; Jenner et al., 2022). Given that bioaccumulation, chronic exposure, or co-exposure with other pollutants could enhance toxic effects over time, including these concentrations provides foundational knowledge for risk assessment and helps establish dose-response relationships that may inform future regulatory thresholds.

3.3. NPL internalization

Evaluating NPL internalization is essential when assessing their potential effects. In this study, internalization of NPLs in HUH-7 cells was confirmed using confocal microscopy (Fig. 3) and quantified by flow cytometry (Fig. 4). Confocal microscopy provided visual confirmation of internalization within HUH-7 cells, while flow cytometry allowed quantitative assessment of internalization levels and comparison across different NPL types and exposure times.

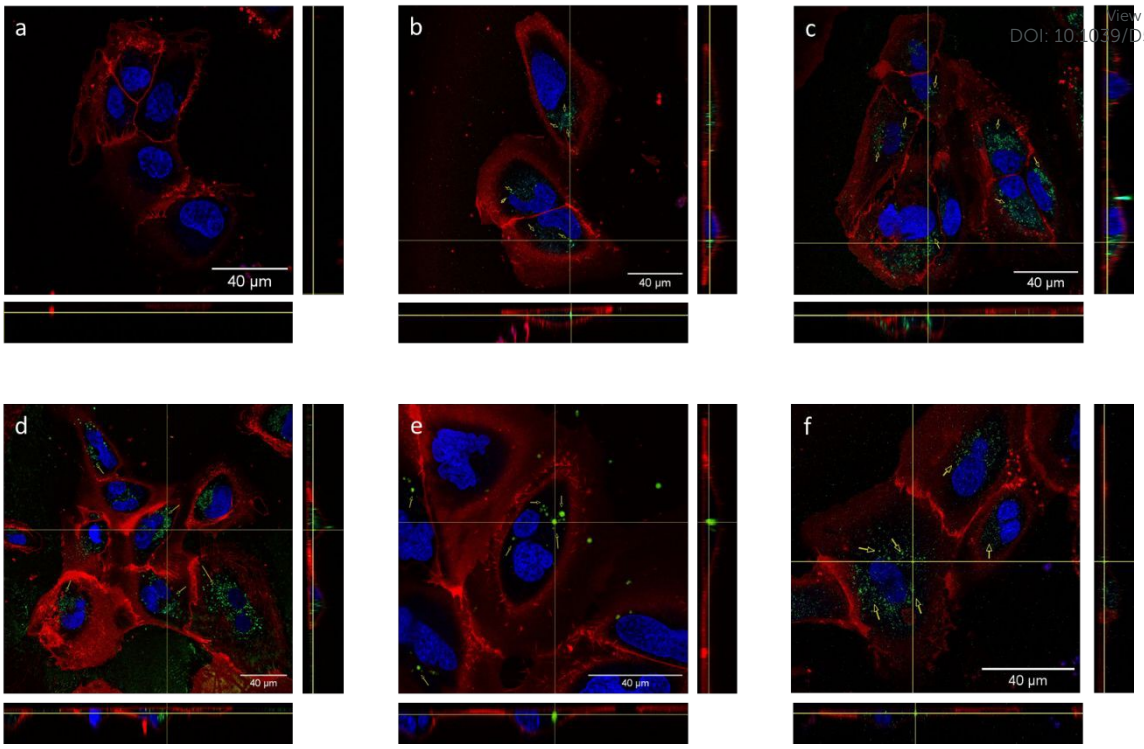

Figure 3. NPLs internalization in HUH-7 cells after 48 h of treatment using fluorescent/labeled NPLs: a) non-treated control, b) f-PS50-NPLs, c) f-cPS50-NPLs, d) f-cPS100-NPLs, e) f-PET-NPLs, and f) f-PLA-NPLs. Cell nuclei are presented in blue, cell membranes in red, and NPLs in green, annotated with yellow arrows. Orthogonal views are included, showing the different NPLs are inside the cell.

The internalization kinetics varied significantly among the NPLs tested. Notably, cPS50-NPLs and PET-NPLs achieved 100% cellular internalization within 1 h, whereas PS50-NPLs took 24 h to reach just 10% internalization. PLA- and cPS100-NPLs exhibited intermediate kinetics, with full internalization observed at 24 and 72 h, respectively. The high internalization rates of the two true-to-life NPLs, representative of secondary environmental NPLs, lend critical insight into their potential relevance. It must be remembered that different fluorophore compounds were used for labelling the different MNPLs and, consequently, differences in detecting the fluorescent signal or intensity could occur. Previous studies have shown that NPL properties such as surface chemistry, size, and functionalization significantly impact cell membrane interactions and uptake efficiency in mammalian cells (Banerjee and Shelver, 2021).

View Article Online
DOI: 10.1039/D5EN00434A

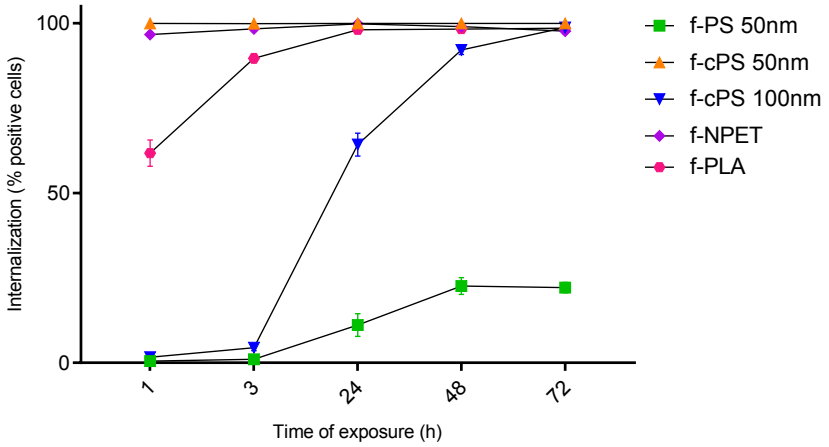

Figure 4. Cellular internalization of fluorescent/labeled NPLs (f-NPLs) by HUH-7 cells after 1, 3, 24, 48, and 72 h of treatment, using flow cytometry. The dynamic of NPLs internalization is presented as a mean ± SEM percentage of fluorescent cells (n=3) in a total of 10,000 scored single cells for each point in time.

The high internalization rates of PET-NPLs and PLA-NPLs may be linked to their hydrophobicity and chemical composition, as similar findings on cellular uptake have been reported in other studies. Furthermore, the rapid internalization of cPS50-NPLs compared to PS50-NPLs highlights the role of surface characteristics over size in determining internalization efficiency, a finding corroborated by previous studies on other cell types that show enhanced internalization rates of carboxylated PS-NPLs compared to their pristine counterparts. Finally, the delayed but pronounced increase in cPS100-NPL internalization observed at 3 h may be explained by the interplay between their surface carboxylation and size. Carboxyl groups promote stronger electrostatic interactions with the cell membrane, while their diameter around 100 nm corresponds to the optimal size range for clathrin- and caveolae-mediated endocytosis, which typically requires longer vesicle formation times compared to smaller particles. Similar delayed uptake kinetics for carboxylated PS NPLs of this size have been reported in other mammalian cell systems (Mazumdar et al., 2021; Banerjee and Shelver, 2021; Martin-Pérez et al., 2024)

Internalization was measured in two ways: as the percentage of cells internalizing NPLs and as the amount of NPLs internalized per cell. The latter measurement is especially relevant, as the degree of NPL accumulation has been shown to modulate

View Article Online
DOI: 10.1039/D5EN00434A

toxicological responses in cells, such as in mouse macrophages (Collin-Faure et al., 2023). Accordingly, we assessed accumulation kinetics in HUH-7 cells (Fig. 5). As shown, cPS50-NPLs not only internalized at the highest rate but also reached the highest accumulation per cell over time. Interestingly, the environmentally representative bioplastic model PLA-NPLs also showed significant accumulation over time.

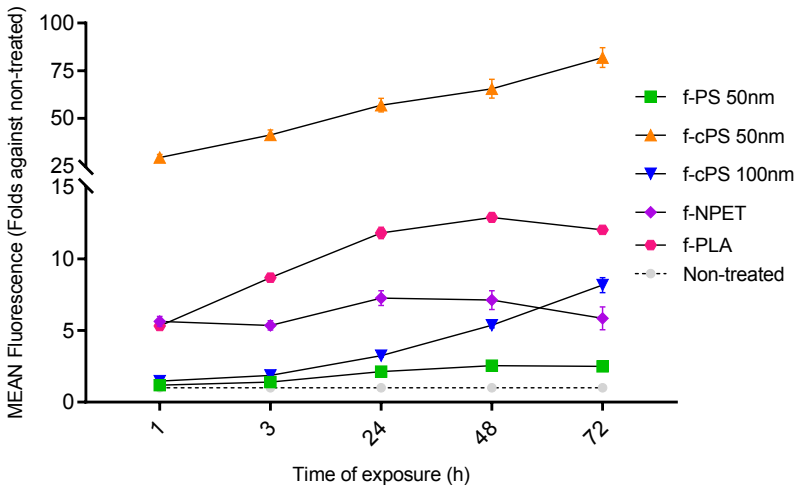

Figure 5. Mean fluorescence signal of HUH-7 cells with fluorescent-NPLs (f-NPLs) internalization after 1, 3, 24, 48, and 72 h of treatment, using flow cytometry. The average fluorescence signal of the HUH-7 cell population that internalized f-NPLs at each time is taken as an indirect measurement of the amount of NPLs inside each cell and normalized as folds against mean fluorescence of the non-treated control. Significant differences ($p \leq 0.001$) in mean fluorescence compared to the non-treated cells were found at all time points when treated with f-cPS50-, f-PET- and f-PLA-NPLs; and 24, 48 and 72 h when treated with f-PS50- and f-cPS50-NPLs. The one-way ANOVA analysis with Dunnett multiple comparisons post-test and 95% confidence was used for the analysis. The graph shows mean ± SEM of fold change against the non-treated control (n=3).

These results support the view that surface characteristics of NPLs significantly influence their internalization kinetics and bioaccumulation potential in cells. Previous studies have found that surface modifications induced by *in vitro* digestion processes can alter PS-NPLs' internalization and toxicological profile in both human liver cells and organisms like zebrafish (Yan et al., 2023). Consequently, this study further evaluates whether internalization rates are associated with distinct toxicological profiles in HUH-7 cells.

View Article Online
DOI: 10.1039/D5EN00434A

3.4. ROS induction

Reactive oxygen species (ROS) generation is a well-established mediator of cellular damage and plays a key role in oxidative stress-related pathologies, including DNA damage and inflammation, both of which are critical in liver disease progression (Sies and Jones, 2020). ROS levels induced by the selected NPLs are shown in Fig. 6. To better isolate the effects of internalized NPLs, we used cell sorting techniques to select only cells with high levels of internalization (Arribas Arranz et al., 2024). This approach helps prevent the lack of ROS effects in non-internalized cells from masking responses in cells with internalized NPLs.

While overall ROS production did not show a statistically significant increase across all time points and treatments, a marked elevation of ROS levels was observed in cells treated with PET-NPLs, suggesting that the higher internalization rate of these NPLs may lead to localized oxidative stress. The ROS induction in this subpopulation aligns with findings from other studies, which report oxidative stress induction in cells with higher particle uptake (Yang et al., 2019; Shen et al., 2022; Das and Medhi, 2023). The pronounced effects of PET observed here are consistent with results from studies in various human cell lines (Villacorta et al., 2022; Tavakolpournegari et al., 2024; Ma et al., 2024).

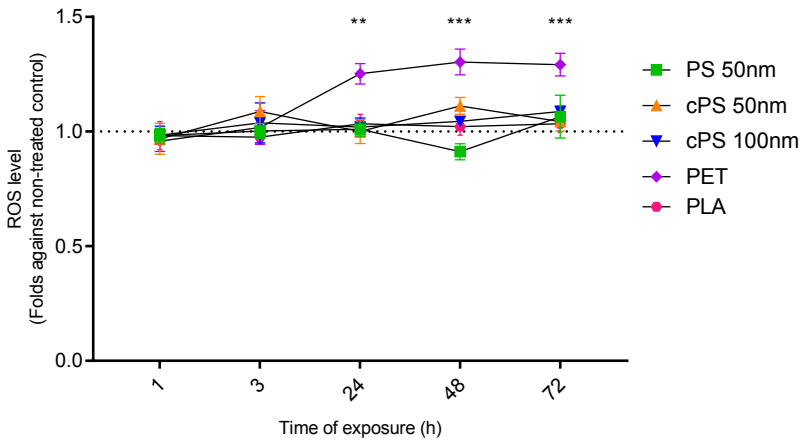

Figure 6. Determination of ROS levels in HUH-7 cells treated for 1, 3, 24, and 48 h with NPLs. Using flow cytometry sorting, 10% of cells with higher internalization were selected and the average signal in the PE channel for the treated cells was compared to that of the non-treated control. Significant differences in mean fluorescence compared to the non-treated cells were determined using the one-way ANOVA analysis, with

Dunnett multiple comparisons post-test and 95% confidence interval (**$p \leq 0.01$, ***$p \leq 0.001$). The graph shows mean ± SEM of fold change against the non-treated control (n=3).

3.5. DNA damage induction

Following the evaluation of oxidative stress potential, we assessed the genotoxic effects of the selected NPLs using the comet assay, which measures both single strand breaks and oxidative DNA base damage. Among the biomarkers for MNPL-induced effects, genotoxicity is especially relevant, given that DNA damage can severely impact cell functionality and, consequently, human health sting (Carbone et al., 2020). Genotoxicity is crucial in evaluating the potential health impacts of emerging pollutants such as MNPLs. Fig. 7 displays the results from the comet assay.

Among the different NPLs assessed, only PLA exposure produced significant genotoxic damage, evidenced by increased DNA strand breaks in treated cells compared to controls. Notably, none of the NPLs tested induced oxidative damage in DNA bases. Our findings are consistent with previous studies, which have shown PLA-NPLs' capacity to cause DNA strand breaks in various cell types. For instance, PEG-b-PLA exposure has been shown to damage DNA in HT-29 and MCF-7 cells (Koňáriková et al., 2023), and PLA induced significant DNA breaks in Calu-3 bronchial epithelial cells, particularly under long-term exposure (García-Rodríguez et al., 2024). Furthermore, *in vivo* studies on *Drosophila* reveal that PLA exposure causes DNA damage in hemocytes, as analogous to lymphocytes in humans (Alaraby et al., 2024).

Though research on the health effects of PLAN-PLs in HUH-7 cells is limited, our findings on their genotoxic potential align with evidence from other cell lines, underscoring the need for further studies into the toxicological profile of this bioplastic degradation product. While the alkaline comet assay used in this case served as a sensitive initial screen for assessing DNA strand breaks and oxidative lesions induced by NPLs exposure in HUH-7 cells, it is important to note that the detection of

chromosome loss or breakage and early double-strand breaks would be valuable for future studies.

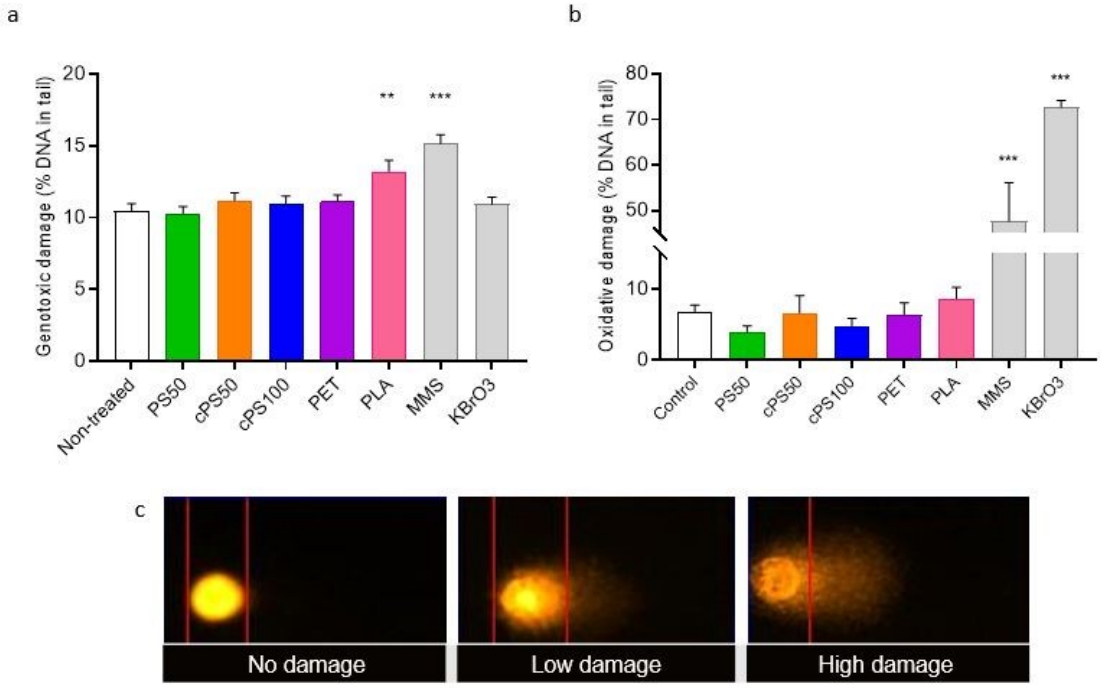

Figure 7. a) Genotoxic and b) oxidative DNA damage in HUH-7 cells treated with the respective NPL during 48 h. The damage was measured with the comet assay and the percentage of DNA in the tail of the comet used to compare against the non-treated control. After the analysis with the one-way ANOVA tests, Dunnett multiple comparisons post-test, and 95% confidence interval (n=3, $^{**}p \leq 0.01$, $^{***}p \leq 0.001$), a significative difference was observed for genotoxic damage in the cells treated with PLA when compared to the non-treated control. Methyl methanesulfonate (MMS) and potassium bromate ($KBrO_3$) were used as positive controls for genotoxic damage and oxidative damage, respectively. Graph shows mean ± SEM percentage of DNA in the tail of the comet (n=3). c) Representative images of DNA damage levels scored for the comet assay.

3.6. Proteome array and cytokine release analysis

The high internalization rates of cPS50-, PLA-, and PET-NPLs can contribute to the induction of cellular damage, which can trigger an inflammatory response. This aligns with the literature suggesting that the surface properties and chemical composition of NPLs strongly dictate their interaction with cellular membranes and their uptake into cells. This interaction type can trigger an immunological response as demonstrated in *ex vivo* studies using human blood cells from healthy donors (Arribas Arranz et al., 2024) and in two human cell lines (A549 and THP-1) (Antonio et al., 2024).

View Article Online
DOI: 10.1039/D5EN00434A

To understand the mechanistic of injury susceptibility and damage responses, as well as the discovery of endpoints of effect, the secretome of HUH7cells was analyzed by using the Human XL Cytokine Array Kit, as a fast, sensitive, and economic tool to detect the relative expression levels of 105 soluble human proteins and evaluate changes in cytokine expression between cells exposed to the selected NPLs and the unexposed controls. Growth medium and cell lysates were analyzed to determine differences in cytokine profiles for cells exposed to the different NPLS. Although no significant results were found in the profile after analyzing cell lysates, the cytokines released to the growth medium revealed key insights into the inflammatory responses triggered by the tested NPLs. Fig. 8 presents those cytokines showing important responses to the exposure. As observed, only PET- and PLA-NPLs were able to induce a certain positive release. For PET-NPL-treated cells significant upregulation was observed in ICAM-1, IL-8, MIF, and Serpin E1, indicating a robust pro-inflammatory and tissue-remodeling response. ICAM-1 is a key marker of immune cell adhesion, which suggests that PET-NPLs may facilitate the recruitment of immune cells, potentially amplifying inflammatory responses in the liver. IL-8 further supports this, as it is a potent chemoattractant for neutrophils, linking PET exposure to neutrophil-mediated inflammation, a common feature in liver injury (Teijeira et al., 2021). Additionally, the increase in MIF (macrophage migration inhibitory factor) suggests that PET-NPLs may enhance macrophage activation, contributing to sustained inflammation. Serpin E1, a regulator of extracellular matrix (ECM) degradation, is associated with tissue remodeling and fibrosis, indicating that PET NPLs may induce early fibrotic responses if exposure persists (Horvatits et al., 2022).

It is also important to note that exposure to PS50-NPLs resulted in a general decrease in cytokine expression relative to non-treated controls. This reductive effect is consistent with emerging research showing that PS-NPs can be relatively inert and immunologically silent in hepatic cell models. For instance, Brandts et al. (2023) demonstrated that PS-NPs largely accumulate in lysosomes of macrophages, as observed also in fish liver cells (Cheng et al., 2022), but do not trigger significant production of ROS or elevation of

View Article Online
DOI: 10.1039/D5EN00434A

inflammatory cytokines such as IL-1β, TNF-α, IL-6, or IL-10 (Weber et al., 2022). Additionally, tissue slice and *in vitro* studies using PS particles revealed downregulation of IL-1β and IL-10 when corona formation is allowed by using medium supplemented with serum, indicating that PS exposure can produce a muted inflammatory phenotype rather than a classical upregulated immune response (Bartucci et al., 2021).

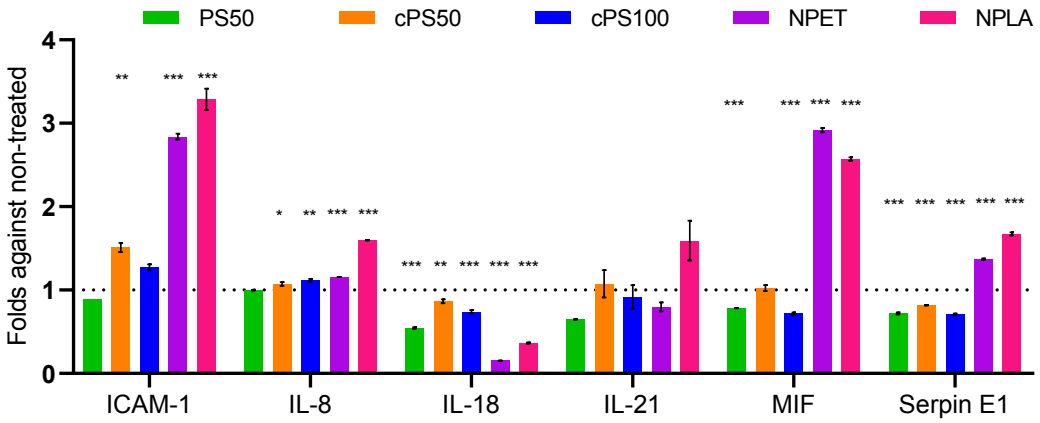

Figure 8. Analysis of growth factors/cytokines released from HUH-7 cells to the growth medium after 48 h of NPLs treatment using the Human Cytokine Array. Expression is represented as folds against the basal level in non-treated cells, represented by the pointed line in the graph. For the statistical analysis, one-way ANOVA test was used with Dunnett multiple comparisons post-test, and 95% confidence interval (n=3, * $p \leq 0.05$ ** $p \leq 0.01$, *** $p \leq 0.001$)

The differential cytokine responses observed between PS50-, PET-, and PLA-NPLs further emphasize that nanoplastic characteristics, such as polymer type and surface properties, can distinctly influence cellular behavior and immune modulation. This agrees with findings from previous studies, where PET- and PLA-NPLs have been shown to elicit strong inflammatory responses, but via distinct pathways depending on their interaction with cellular receptors and their internalization rates (Arribas Arrranz et al., 2024; García-Rodríguez et al., 2024). Furthermore, the response induced by PET-NPL and PLA-NPL exposures in liver HUH-7 cells reinforce the view that some characteristics of MNPLs can play pivotal roles in targeting liver as reviewed by different authors (Banerjee and Shelver, 2021; Yin et al., 2022; Haldar et al., 2023).

To further investigate intracellular responses, cytokine expression was also measured in supernatant and cell lysates of HUH-7 cells exposed to PET- and PLA-NPLs for 48 h, with an additional 12-h LPS treatment to mimic inflammatory stimuli (Fig. 9). Although no significant difference was observed in the supernatant profile, both nanoplastics induced significant upregulation of IL-6, IL-8, IL-18, and Serpin E1 in the lysate of cells exposed under this combination of treatments. This response suggests that PET and PLA not only trigger cytokine secretion but also modulate intracellular signaling pathways involved in immune and inflammatory responses.

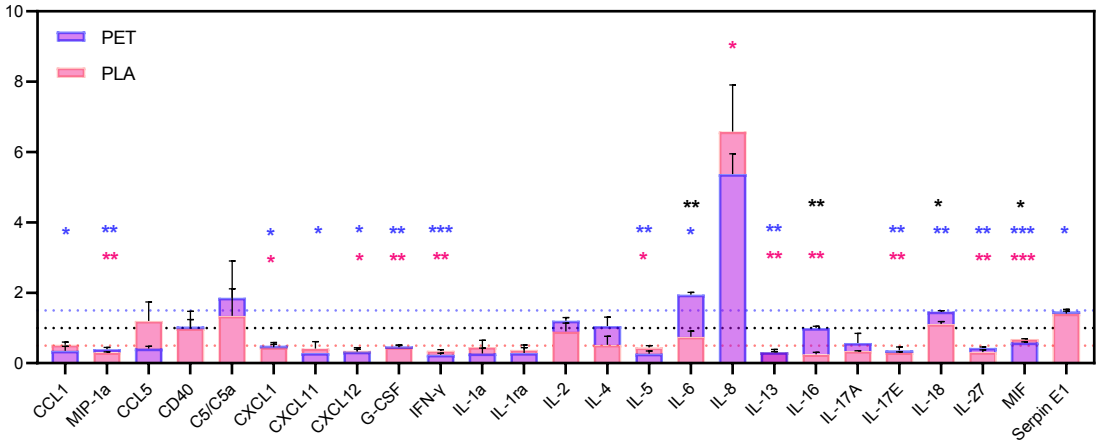

Figure 9. Analysis of growth factors/cytokines in cell lysis from HUH-7 cells with higher PET and PLA internalization after 48 h and a 12 h treatment with 1 µg/mL LPS. Expression is represented as folds against the basal level in non-treated cells, represented by the pointed black line in the graph. Cytokines with lower than 0.5 or higher than 1.5 folds compared to the non-treated cells, were included in the analysis. One-way ANOVA analysis, with Dunnett multiple comparisons post-test and 95% confidence interval was used for the analysis (*$p \leq 0.05$, **$p \leq 0.01$, ***$p \leq 0.001$). The graph shows mean ± SEM of fold change against the non-treated control (n=3), with significant differences between NPET and the control in blue *, between the NPLA and the control in red, and between both NPLs in black.

Results show that for PET-treated cells, the combination of PET and LPS resulted in significantly elevated levels of IL-6, IL-8, IL-18, and Serpin E1. The sharp increase in IL-6 and IL-8 reflects a potent intracellular inflammatory response, with IL-8 promoting neutrophil chemotaxis and IL-6 driving acute-phase responses (Shen et al., 2022). IL-18 further contributes to this inflammatory cascade by promoting the production of IFN-γ, a key cytokine in the immune response to infection (Dinarello et al., 2013). The

upregulation of Serpin E1 suggests that PET, especially in combination with LPS, may also stimulate pathways related to extracellular matrix remodeling and fibrosis. Thus, the combined PET-NPLs and LPS treatment appears to exacerbate inflammatory and fibrotic responses, reflecting a synergistic effect between environmental pollutants and microbial stimuli, which could increase the risk of chronic liver inflammation and fibrosis.

For PLA-treated cells, intracellular increases of C5, IL-8, and Serpin E1 were observed after the combined exposure to PLA-NPLs and LPS. The elevation of C5 indicates activation of the complement system, which plays a significant role in inflammation and immune cell recruitment (Strey et al., 2003). The increased levels of IL-8 also suggest that neutrophil recruitment is a key response to PLA-NPLs exposure, particularly in the presence of LPS. Interestingly, many other intracellular cytokines were downregulated (below 0.5-fold) compared to the control, suggesting that PLA-NPLs may primarily activate complement and neutrophil-mediated pathways without broadly stimulating other intracellular inflammatory responses. The concurrent increase in Serpin E1 supports the idea that PLA, like PET-NPLs, may induce tissue remodeling and fibrotic changes over time. Interestingly, most of the other cytokines in PLA-treated lysates were expressed at levels significantly below the control, suggesting a suppression of intracellular pro-inflammatory responses for certain cytokines. This could indicate that while PLA-NPLs induces extracellular pro-inflammatory and immune-activating cytokines, its intracellular effects may be more focused on complement activation and neutrophil recruitment, rather than broad pro-inflammatory signaling.

The addition of LPS after 48 h of nanoplastic exposure provides important insights into how environmental nanoplastics and microbial products can synergize amplifying liver inflammation. LPS is a known activator of the Toll-like receptor 4 (TLR4) pathway, which stimulates the release of pro-inflammatory cytokines and chemokines (Akira et al., 2006). When combined with nanoplastics like PET or PLA, the presence of LPS appears to amplify inflammatory signaling, resulting in the elevated production of cytokines such as IL-6, IL-8, IL-18, and C5, depending on the nanoplastic type. Thus, the amplified

View Article Online
DOI: 10.1039/D5EN00434A

inflammatory response observed after co-treatment with LPS suggests that nanoplastics like PET- and PLA-NPLs could prime hepatocytes for heightened inflammatory sensitivity. This raises concerns about synergistic effects between environmental pollutants and microbial products, which could exacerbate liver inflammation and contribute to the development of chronic liver conditions, including non-alcoholic fatty liver disease (NAFLD) and cirrhosis (Das, 2023). The presence of ICAM-1 and IL-6 as key mediators highlights the potential for inflammatory crosstalk between NPL exposure and immune system activation, which could accelerate the progression of liver disease. Moreover, the differential cytokine responses between PLA-NPLs and PET-NPLs suggest that these nanoplastics not only affect oxidative stress pathways but also modulate the immune response in different ways. The strong association between PLA-NPL genotoxicity and IL-18 expression, points toward the activation of pathways involved in cellular damage repair and, possibly, to early fibrotic changes, while PET's induction of IL-6, IL-8, and ICAM-1 suggests a more acute pro-inflammatory response, potentially setting the stage for chronic inflammation if exposure were prolonged.

It is important to address the genotoxic and pro-inflammatory responses in HUH-7 cells after exposure to PLA-NPLs, considering that PLA is widely regarded as a safer and more environmentally friendly bioplastic. However, recent studies have challenged this perception showing these NPLs induce oxidative stress, DNA damage, and inflammatory gene activation *in vivo*, such as in *Drosophila melanogaster* larvae models (Alaraby et al., 2024). *In vitro* studies also demonstrate that UV-aged PLA films release surface-modified nanoplastics with increased reactivity, capable of inducing cytotoxicity and inflammation comparable to that of conventional plastics (Wu et al., 2025). The effects have been linked to changes in surface chemistry, such as the appearance of carbonyl or hydroxyl groups, as well as the presence of residual monomers or additives used in commercial PLA formulations. These findings align with the results of the present study and reinforce that bioplastics like PLA can have cytotoxic effects and should be assessed with the same level of scrutiny as conventional petroleum-based plastics when

View Article Online
DOI: 10.1039/D5EN00434A

considering potential impacts on human and environmental health. Future studies will be essential to evaluate how environmental degradation, aging, or additive leaching may modulate the toxicity profile of PLA-based materials.

4. Conclusion

This study underscores the importance of evaluating the specific characteristics of nanoplastics (NPLs), such as polymer type, surface charge, and size, when assessing their biological effects. Determining internalization ability and kinetics over time are essential parameters for understanding NPLs' biological impact. Significant differences in cell uptake were observed, notably highlighting the influence of surface charge, as carboxylated PS-NPLs showed high internalization efficiency compared to their pristine counterparts. The robust internalization of PET- and PLA-NPLs may be attributed to surface modifications introduced during their preparation, underscoring the need for realistic environmental analogs in toxicological studies.

Interestingly, efficient internalization alone does not necessarily predict harmful cellular outcomes, as evidenced by pristine PS50-NPLs, which demonstrated high internalization yet minimal adverse effects. This indicates that a specific cell line, such as HUH-7, may exhibit distinct responses to different NPLs, with notable implications for liver health concerning chronic inflammation, fibrosis, and carcinogenesis risk. In our study, PET-NPLs and PLA-NPLs notably induced a range of responses in hepatic cells, including ROS production, genotoxicity, and cytokine release, highlighting the significance of true-to-life MNPLs as representatives of environmentally relevant secondary MNPLs.

Further research is needed to investigate the long-term effects of these nanoplastics, including their internalization kinetics, in hepatic cells and their potential role in liver disease progression.

View Article Online
DOI: 10.1039/D5EN00434A

Author contributions

All authors contributed to the article and approved the submitted version.

Conceptualization: RM and AH; Funding acquisition: AH; Investigation: MMR, AV, JAA, JMP, SP, RE, and IB; Methodology: MMR and AV; Resources: JFF; Supervision: AH and RM; Writing –original draft: MMR; Writing –review and editing: RM and AH.

Acknowledgments

MMR and JMP hold Ph.D. fellowships from the Generalitat de Catalunya. AV was supported by a Ph.D. fellowship from the National Agency for Research and Development (ANID); Nucleo de Investigación en Ciencias Biológicas., CONICYT PFCHA/DOCTORADO BECAS CHILE/202072210237. IB (Academic record 2023 BP 00212) was granted with a Beatriu de Pinós Postdoctoral Program from the Secretariat of Universities and Research of the Department of Business and Knowledge of the Government of Catalunya. AH was granted an ICREA ACADEMIA award. This project (Plasticheal) has received funding from the European Union's Horizon 2020 research and innovation programme under grant agreement No 965196. This work was partially supported by the Spanish Ministry of Science and Innovation [PID2020-116789, RB-C43] and the Generalitat de Catalunya (2021-SGR-00731).

Declaration of Competing Interests

The authors declare that they have no known competing financial interests or personal relationships that could have appeared to influence the work reported in this paper.

View Article Online
DOI: 10.1039/D5EN00434A

References

Akira S, Uematsu S, Takeuchi O. Pathogen recognition and innate immunity. Cell. 2006; 124(4):783–801. doi: 10.1016/j.cell.2006.02.015.

Alaraby M, Abass D, Farre M, Hernández A, Marcos, R. Are bioplastics safe? Hazardous effects of polylactic acid (PLA) nanoplastics in *Drosophila*. Sci Total Environ. 2024; 919:170592. doi: 10.1016/j.scitotenv.2024.170592.

Ali N, Katsouli J, Marczylo EL, Gant TW, Wright S, Bernardino de la Serna J. The potential impacts of micro-and-nano plastics on various organ systems in humans. EBioMedicine. 2024; 99:104901. doi: 10.1016/j.ebiom.2023.104901.

Alqahtani S, Alqahtani S, Saquib Q, Mohiddin F. Toxicological impact of microplastics and nanoplastics on humans: understanding the mechanistic aspect of the interaction. Front Toxicol. 2023; 5:1193386. doi: 10.3389/ftox.2023.1193386.

Antonio L, Visalli G, Facciolà A, Saija C, Bertuccio MP, Baluce B, Celesti C, Iannazzo D, Di Pietro A. Sterile inflammation induced by respirable micro and nano polystyrene particles in the pathogenesis of pulmonary diseases. Toxicol Res (Camb). 2024; 13(5):tfae138. doi: 10.1093/toxres/tfae138.

Arribas Arranz J, Villacorta A, Rubio L, García-Rodríguez A, Sánchez G, Llorca M, Farre M, Ferrer JF, Marcos R, Hernández A. Kinetics and toxicity of nanoplastics in *ex vivo* exposed human whole blood as a model to understand their impact on human health. Sci Total Environ. 2024; 948:174725. doi: 10.1016/j.scitotenv.2024.174725.

Banaei G, García-Rodríguez A, Tavakolpournegari A, Martín-Pérez J, Villacorta A, Marcos R, Hernández A. The release of polylactic acid nanoplastics (PLA-NPLs) from commercial teabags. Obtention, characterization, and hazard effects of true-to-life PLA-NPLs. J Hazard Mater. 2023; 458:131899. doi: 10.1016/j.jhazmat.2023.131899.

Banerjee A, Shelver WL. Micro- and nanoplastic induced cellular toxicity in mammals: A review. Sci Total Environ. 2021; 755:142518. doi: 10.1016/j.scitotenv.2020.142518.

Bartucci R, van der Meer AZ, Boersma YL, Olinga P, Salvati A. Nanoparticle-induced inflammation and fibrosis in *ex vivo* murine precision-cut liver slices and effects of nanoparticle exposure conditions. Arch Toxicol. 2021; 95(4):1267–85. doi: 10.1007/s00204-021-02992-7.

Bhattacharjee S. DLS and zeta potential - What they are and what they are not? J Control Release. 2016; 235:337–51. doi: 10.1016/j.jconrel.2016.06.017.

Brandts I, Solà R, Garcia-Ordoñez M, Gella A, Quintana A, Martin B, Esteve-Codina A, Teles M, Roher N. Polystyrene nanoplastics target lysosomes interfering with lipid metabolism through the PPAR system and affecting macrophage functionalization. Environ Sci Nano. 2023; 10(9):2245–58. doi: 10.1039/d2en01077a.

Carbone M, Arron ST, Beutler B, Bononi A, Cavenee W, Cleaver JE, Croce Jr CM, *et al.* Tumour predisposition and cancer syndromes as models to study gene-environment interactions. Nat Rev Cancer. 2020; 20(9):533–49. doi: 10.1038/s41568-020-0265-y.

Catarino A, Patsiou D, Summers S, Everaert G, Henry T, Gutierrez T. Challenges and recommendations in experimentation and risk assessment of nanoplastics in aquatic organisms. Trac-Trends Anal Chem. 2023; 167:117262. doi: 10.1016/j.trac.2023.117262.

Chen G, Feng Q, Wang J. Mini-review of microplastics in the atmosphere and their risks to humans. Sci Total Environ. 2020; 703:135504. doi: 10.1016/j.scitotenv.2019.135504.

Cheng H, Duan Z, Wu Y, Wang Y, Zhang H, Shi Y, Zhang H, Wei Y, Sun H. Immunotoxicity responses to polystyrene nanoplastics and their related mechanisms in the liver of zebrafish (*Danio rerio*) larvae. Environ Int. 2022; 161:107128. doi: 10.1016/j.envint.2022.107128.

Collin-Faure V, Vitipon M, Torres A, Tanyeres O, Dalzon B, Rabilloud T. The internal dose makes the poison: higher internalization of polystyrene particles induce increased perturbation of macrophages. Front Immunol. 2023; 14:1092743. doi: 10.3389/fimmu.2023.1092743.

Collins A, Møller P, Gajski G, Vodenková S, Abdulwahed A, Anderson D, Bankoglu EE, *et al.* Measuring DNA modifications with the comet assay: a compendium of protocols. Nat Protoc. 2023; 18(3):929–89. doi: 10.1038/s41596-022-00754-y.

Das A. The emerging role of microplastics in systemic toxicity: Involvement of reactive oxygen species (ROS). Sci Total Environ. 2023; 895:165076. doi: 10.1016/j.scitotenv.2023.165076.

Das P, Medhi S. Role of inflammasomes and cytokines in immune dysfunction of liver cirrhosis. Cytokine. 2023; 170:156347. doi: 10.1016/j.cyto.2023.156347.

Dinarello CA, Novick D, Kim S, Kaplanski G. Interleukin-18 and IL-18 binding protein. Front Immunol. 2013; 4:289. doi: 10.3389/fimmu.2013.00289.

Domenech J, Villacorta A, Ferrer J, Llorens-Chiralt R, Marcos R, Hernández A, Catalán J. *In vitro* cell-transforming potential of secondary polyethylene terephthalate and polylactic acid nanoplastics. J Hazard Mater. 2024; 469:134030. doi: 10.1016/j.jhazmat.2024.134030.

EC. European Commission Recommendation of 10 June 2022 on the definition of nanomaterial; 2022. Retrieved from https://eur-lex.europa.eu/legal-content/EN/TXT/PDF/?uri=CELEX:32022H0614(01).

Enfrin M, Dumée LF, Lee J. Nano/microplastics in water and wastewater treatment processes – Origin, impact and potential solutions. Water Res. 2019; 161:621–38. doi: 10.1016/j.watres.2019.06.049

Fan X, Wei X, Hu H, Zhang B, Yang D, Du H, Zhu R, Sun X, Oh Y, Gu N. Effects of oral administration of polystyrene nanoplastics on plasma glucose metabolism in mice. Chemosphere. 2022; 288:132607. doi: 10.1016/j.chemosphere.2021.132607.

García-Rodríguez A, Gutiérrez J, Villacorta A, Arribas Arranz J, Romero-Andrada I, Lacoma A, Marcos R, Hernández A, Rubio L. Polylactic acid nanoplastics (PLA-NPLs) induce adverse effects on an *in vitro* model of the human lung epithelium: The Calu-3 air-liquid interface (ALI) barrier. J Hazard Mater. 2024; 475:134900. doi: 10.1016/j.jhazmat.2024.134900.

Ge Y, Yang S, Zhang T, Wan X, Zhu Y, Yang F, Yin L, Pu Y, Liang G. The hepatotoxicity assessment of micro/nanoplastics: A preliminary study to apply the adverse outcome pathways. Sci Total Environ. 2023; 902:165659. doi: 10.1016/j.scitotenv.2023.165659.

Geyer R, Jambeck JR, Law KL. Production, use, and fate of all plastics ever made. Sci Adv. 2017; 3(7):e1700782. doi: 10.1126/sciadv.1700782.

Haldar S, Yhome N, Muralidaran Y, Rajagopal S, Mishra P. Nanoplastics toxicity specific to liver in inducing metabolic dysfunction—a comprehensive review. Genes. 2023; 14(3):590. doi: 10.3390/genes14030590.

He Y, Li J, Chen J, Miao X, Li G, He Q, Xu H, Li H, Wei Y. Cytotoxic effects of polystyrene nanoplastics with different surface functionalization on human HepG2 cells. Sci Total Environ. 2020; 723:138180. doi: 10.1016/j.scitotenv.2020.138180.

Horvatits T, Tamminga M, Liu B, Sebode M, Carambia A, Fischer L, Püschel K, Huber S, Fischer EK. Microplastics detected in cirrhotic liver tissue. EBioMedicine. 2022; 82:104147. doi: 10.1016/j.ebiom.2022.104147.

Jenner LC, Rotchell JM, Bennett RT, Cowen M, Tentzeris V, Sadofsky LR. Detection of microplastics in human lung tissue using μFTIR spectroscopy. Sci Total Environ. 2022; 831:154907. doi: 10.1016/j.scitotenv.2022.154907.

Johnson LM, Mecham JB, Krovi SA, Moreno Caffaro MM, Aravamudhan S, Kovach AL, Fennell TR, Mortensen NP. Fabrication of polyethylene terephthalate (PET) nanoparticles with fluorescent tracers for studies in mammalian cells. Nanoscale Adv. 2021; 3(2):339–46. doi: 10.1039/d0na00888e.

Jouan E, Le Vée M, Denizot C, Parmentier Y, Fardel O. Drug transporter expression and activity in human hepatoma HuH-7 cells. Pharmaceutics. 2016; 9(1):3. doi: 10.3390/pharmaceutics9010003.

Khan A, Jia Z. Recent insights into uptake, toxicity, and molecular targets of microplastics and nanoplastics relevant to human health impacts. IScience. 2023; 26(2):106061. doi: 10.1016/j.isci.2023.106061.

Kooi M, Koelmans AA. Simplifying microplastic via continuous probability distributions for size, shape, and density. Environ Sci Technol Lett. 2019; 6(9):551–57. doi: 10.1021/acs.estlett.9b00379

Koňáriková K, Girašková G, Žitňanová I, Dvořáková M, Rollerová E, Scsuková S, Bizik J, Janubová M, Muchová J. Biological analyses of the effects of TiO_2 and PEG-b-PLA nanoparticles on three-dimensional spheroid-based tumor. Physiol Res. 2023; 72(S3):S257–S266. doi: 10.33549/physiolres.935152.

Ma L, Wu Z, Lu Z, Yan L, Dong X, Dai Z, Sun R, Hong P, Zhou C, Li C. Differences in toxicity induced by the various polymer types of nanoplastics on HepG2 cells. Sci Total Environ. 2024; 918:170664. doi: 10.1016/j.scitotenv.2024.170664.

Marfella R, Prattichizzo F, Sardu C, Fulgenzi G, Graciotti L, Spadoni T, D'Onofrio N, Scisciola L, La Grotta R, Frigé C, Pellegrini V, Municinò M, Siniscalchi M, Spinetti F, Vigliotti G, Vecchione C, Carrizzo A, Accarino G, Squillante A, et al. Microplastics and nanoplastics in atheromas and cardiovascular events. N Engl J Med. 2024; 390(10):900910. doi: 10.1056/nejmoa2309822.

Martin LM, Gan N, Wang E, Merrill M, Xu W. Materials, surfaces, and interfacial phenomena in nanoplastics toxicology research. Environ Pollut. 2022; 292:118442. doi: 10.1016/j.envpol.2021.118442.

Martín-Pérez J, Villacorta A, Banaei G, Morataya-Reyes M, Tavakolpournegari A, Marcos R, Hernández A, García-Rodriguez A. Hazard assessment of nanoplastics is driven by their surface-functionalization. Effects in human-derived primary endothelial cells. Sci Total Environ. 2024; 934:173236. doi: 10.1016/j.scitotenv.2024.173236.

Materić D, Holzinger R, Niemann H. Nanoplastics and ultrafine microplastic in the Dutch Wadden Sea – he hidden plastics debris? Sci Total Environ. 2022: 846:157371. doi: 10.1016/j.scitotenv.2022.157371.

Mazumdar S, Chitkara D, Mittal A. Exploration and insights into the cellular internalization and intracellular fate of amphiphilic polymeric nanocarriers. Acta Pharm Sin B. 2021; 11(4):903–24. doi: 10.1016/j.apsb.2021.02.019.

Mills CL, Savanagouder J, de Almeida Monteiro Melo Ferraz M, Noonan MJ. The need for environmentally realistic studies on the health effects of terrestrial microplastics. Microplast Nanoplast. 2023; 3(1):11. doi: 10.1186/s43591-023-00059-1.

Nazrin A, Sapuan SM, Zuhri MYM. Mechanical, physical and thermal properties of sugar palm nanocellulose reinforced thermoplastic starch (TPS)/poly (lactic acid) (PLA) blend bionanocomposites. Polymers. 2020; 12(10):2216. doi: 10.3390/polym12102216.

Onugwu AL, Nwagwu CS, Onugwu OS, Echezona AC, Agbo CP, Ihim SA, Emeh P, Nnamani PO, Attama AA, Khutoryanskiy VV. Nanotechnology based drug delivery systems for the treatment of anterior segment eye diseases. J Control Release. 2023; 354:465–88. doi: 10.1016/j.jconrel.2023.01.018.

Paul MB, Stock V, Cara-Carmona J, Lisicki E, Shopova S, Fessard V, Braeuning A, Sieg H, Böhmert L. Micro- and nanoplastics -current state of knowledge with the focus on oral uptake and toxicity. Nanoscale Adv. 2020; 2(10):4350–67. doi: 10.1039/d0na00539h.

Pironti C, Notarstefano V, Ricciardi M, Motta O, Giorgini E, Montano L. First evidence of microplastics in human urine, a preliminary study of intake in the human body. Toxics. 2022; 11(1):40. doi: 10.3390/toxics11010040.

Pradel A, Catrouillet C, Gigault J. The environmental fate of nanoplastics: What we know and what we need to know about aggregation. NanoImpact. 2023; 29:100453. doi; 10.1016/j.impact.2023.100453.

Ragusa A, Svelato A, Santacroce C, Catalano P, Notarstefano V, Carnevali O, Papa F, Rongioletti MCA, Baiocco F, Draghi S, D'Amore E, Rinaldo D, Matta M, Giorgini E. Plasticenta: First evidence of microplastics in human placenta. Environ Int. 2021; 146:106274. doi: 10.1016/j.envint.2020.106274.

Schwabl P, Köppel S, Königshofer P, Bucsics T, Trauner M, Reiberger T, Liebmann B. Detection of various microplastics in human stool: a prospective case series. Ann Intern Med. 2019; 171(7):453–7. doi: 10.7326/M19-0618.

Sendra M, Pereiro P, Yeste M, Mercado L, Figueras A, Novoa B. Size matters: Zebrafish (*Danio rerio*) as a model to study toxicity of nanoplastics from cells to the whole organism. Environ Pollut. 2021; 268:115769. doi: 10.1016/j.envpol.2020.115769.

Shen R, Yang K, Cheng X, Guo C, Xing X, Sun H, Liu D, Liu X, Wang D. Accumulation of polystyrene microplastics induces liver fibrosis by activating cGAS/STING pathway. Environ Pollut. 2022; 300:118986. doi: 10.1016/j.envpol.2022.118986.

Shi Q, Tang J, Liu R, Wang L. Toxicity *in vitro* reveals potential impacts of microplastics and nanoplastics on human health: A review. Crit Rev Env Sci Technol. 2021; 52(21):3863–95. doi: 10.1080/10643389.2021.1951528.

Sies H, Jones DP. Reactive oxygen species (ROS) as pleiotropic physiological signalling agents. Nat Rev Mol Cell Biol. 2020; 21:363–83. doi: 10.1038/s41580-020-0230-3.

Strey CW, Markiewski M, Mastellos D, Tudoran R, Spruce LA, Greenbaum LE, Lambris JD. The proinflammatory mediators C3a and C5a are essential for liver regeneration. J Exp Med. 2003; 198(6):913–23. doi: 10.1084/jem.20030374.

Tavakolpournegari A, Annangi B, Villacorta A, Banaei G, Martin J, Pastor S, Marcos R, Hernández A. Hazard assessment of different-sized polystyrene nanoplastics in hematopoietic human cell lines. Chemosphere. 2023; 325:138360. doi: 10.1016/j.chemosphere.2023.138360.

Teijeira A, Garasa S, Ochoa M del C, Cirella A, Olivera I, Glez-Vaz J, Andueza MP, Migueliz I, Alvarez M, Rodríguez-Ruiz ME, Rouzaut A, Berraondo P, Sanmamed MF, Perez Gracia JL, Melero I. Differential interleukin-8 thresholds for chemotaxis and netosis in human neutrophils. Eur J Immunol. 2021; 51(9):2274–80. doi: 10.1002/eji.202049029.

Vasse GF, Melgert BN. Microplastic and plastic pollution: impact on respiratory disease and health. Eur Respir Rev. 2024; 33(172):230226. doi: 10.1183/16000617.0226-2023.

Vethaak AD, Legler J. Microplastics and human health. Science. 2021; 371(6530):672-4. doi: 10.1126/science.abe5041.

Villacorta A, Rubio L, Alaraby M, López-Mesas M, Fuentes-Cebrian V, Moriones OH, Marcos R, Hernández A. A new source of representative secondary PET nanoplastics. Obtention, characterization, and hazard evaluation. J Hazard Mater. 2022; 439:129593. doi: 10.1016/j.jhazmat.2022.129593.

Villacorta A, Vela L, Morataya-Reyes M, Llorens-Chiralt R, Rubio L, Alaraby M, Marcos R, Hernández A. Titanium-doped PET nanoplastics of environmental origin as a true-to-life model of nanoplastic. Sci Total Environ. 2023; 880:163151. doi: 10.1016/j.scitotenv.2023.163151.

Villacorta A, Cazorla-Ares C, Fuentes-Cebrian V, Valido IH, Vela L, Carrillo-Navarrete F, Morataya-Reyes M, Mejia-Carmona K, Pastor S, Velázquez A, Arribas Arranz J, Marcos R, López-Mesas M, Hernández A. Fluorescent labeling of micro/nanoplastics for biological applications with a focus on "true-to-life" tracking. J Hazard Mater. 2024; 476:135134. doi: 10.1016/j.jhazmat.2024.135134.

Wang X, Deng K, Zhang P, Chen Q, Magnuson JT, Qiu W, Zhou Y. Microplastic-mediated new mechanism of liver damage: From the perspective of the gut-liver axis. Sci Total Environ. 2024; 919:170962. doi: 10.1016/j.scitotenv.2024.170962.

Weber A, Schwiebs A, Solhaug H, Stenvik J, Nilsen AM, Wagner M, Relja B, Radeke HH. Nanoplastics affect the inflammatory cytokine release by primary human monocytes and dendritic cells. Environ Int. 2022; 163:107173. doi: 10.1016/j.envint.2022.107173.

Wright SL, Kelly FJ. Plastic and human health: a micro issue? Environ Sci Technol. 2017; 51(12):6634–47. doi: 10.1021/acs.est.7b00423.

Wu X, Zhang H, Chen J, Tan F, Cai R, Wang Y. Photoaging promotes toxic micro/nanoplastics release from PLA/PBAT biodegradable plastic in gastrointestinal condition. Environ Health. 2025; 3(5):446-57. doi: 10.1021/envhealth.4c00209.

Yan N, Wang Y, Wong TY, Hu Y, Xu H, Parodi A, Pan K, Liu J, Lam H, Tang BZ, Jianbo Shi J. Surface topography of nanoplastics modulates their internalization and toxicity in liver cells. Environ Sci Nano. 2023; 10:2685. doi: 10.1039/D3EN00347G.

Yang YF, Chen CY, Lu TH, Liao CM. Toxicity-based toxicokinetic/ toxicodynamic assessment for bioaccumulation of polystyrene microplastics in mice. J Hazard Mater. 2019; 366:703–13. doi: 10.1016/j.jhazmat.2018.12.048.

Yee MSL, Hii LW, Looi CK, Lim WM, Wong SF, Kok YY, Tan BK, Wong CY, Leong CO. Impact of microplastics and nanoplastics on human health. Nanomaterials. 2021; 11(2):496. doi: 10.3390/nano11020496.

Yin J, Ju Y, Qian H, Wang J, Miao X, Zhu Y, Zhou L, Ye L. Nanoplastics and microplastics may be damaging our livers. Toxics. 2022; 10(10):586. doi: 10.3390/toxics10100586.

Zhang Y, Kang S, Allen S, Allen D, Gao T, Sillanpää M. Atmospheric microplastics: A review on current status and perspectives. Earth-Sci Rev. 2020; 203:103118. doi: 10.1016/j.earscirev.2020.103118.

Zitouni N, Bousserrhine N, Missawi O, Boughattas I, Chèvre N, Santos R, Belbekhouche S, Alphonse V, Tisserand F, Balmassiere L, Dos Santos SP, Mokni M, Guerbej H, Banni M. Uptake, tissue distribution and toxicological effects of environmental microplastics in early juvenile fish *Dicentrarchus labrax*. J Hazard Mater. 2021; 403:124055. doi: 10.1016/j.jhazmat.2020.124055.

Data Availability Statement

View Article Online
DOI: 10.1039/D5EN00434A

Data will be available under request.